

STRONG EVIDENCE FOR GAMMA-RAY LINES FROM THE INNER GALAXY

MENG SU^{1,3}, DOUGLAS P. FINKBEINER^{1,2}*Draft version January 14, 2019*

ABSTRACT

Using 3.7 years of *Fermi*-LAT data, we examine the diffuse gamma-ray emission in the inner Galaxy in the energy range $80 \text{ GeV} < E < 200 \text{ GeV}$. We find a diffuse gamma-ray feature at $\sim 110 \text{ GeV}$ to $\sim 140 \text{ GeV}$ which can be modeled by a $\lesssim 4^\circ$ FWHM Gaussian in the Galactic center. The morphology is not correlated with the recently discovered *Fermi* bubbles. The null hypothesis of zero intensity is ruled out by 5.0σ (3.7σ with trials factor). The energy spectrum of this structure is consistent with a single spectral line (at energy $127.0 \pm 2.0 \text{ GeV}$ with $\chi^2 = 4.48$ for 4 d.o.f.). A pair of lines at $110.8 \pm 4.4 \text{ GeV}$ and $128.8 \pm 2.7 \text{ GeV}$ provides a marginally better fit (with $\chi^2 = 1.25$ for 2 d.o.f.). The total luminosity of the structure is $(3.2 \pm 0.6) \times 10^{35} \text{ erg/s}$, or $(1.7 \pm 0.4) \times 10^{36} \text{ photons/sec}$. The observation is compatible with a 142 GeV WIMP annihilating through γZ and γh for $m_h \sim 130 \text{ GeV}$, as in the “Higgs in Space” scenario.

Subject headings: gamma rays — diffuse emission — milky way — dark matter

1. INTRODUCTION

Although various cosmological and astrophysical observations provide compelling evidence for dark matter (DM), which constitutes $\sim 80\%$ of the matter in the Universe, we still know little about its intriguing nature (e.g. Bertone et al. 2005; Hooper & Profumo 2007). Among a forest of dark matter models, stable Weakly Interacting Massive Particles (WIMP) have been predicted in many extensions of the Standard Model of particle physics (e.g. Bergström 2000). The WIMP with the virtues of weak scale masses and couplings is an excellent dark matter particle candidate which can annihilate into high energy gamma-rays (e.g. Bergström et al. 1998). The inner Galaxy provides one of the most promising regions on the sky to search for WIMP annihilation produced gamma rays (Ackermann et al. 2011; Abramowski et al. 2011; Gondolo & Silk 1999). The expected relatively higher annihilation rate due to higher dark matter particle density provides a potential window to identify any non-gravitational dark matter signatures.

The “smoking-gun” signal of annihilating dark matter would be a monochromatic gamma-ray line (or lines) in a region of high dark matter density, either in local dwarf galaxies or in the Galactic center. This line could be produced by dark matter decays or annihilations into two photons, or two-body final states involving one photon plus a Higgs boson, Z boson, or other chargeless non-SM particle. In most models, dark matter does not annihilate directly to photons, but in models

where it annihilates to charged lepton pairs, there may be loop interactions that produce photons in two-body final states, yielding spectral lines. These lines can provide a signature of dark matter even in a complicated astrophysical environment, because no known astrophysical process produces gamma-ray lines at $E \gg 1 \text{ GeV}$. However, these loop processes would be suppressed by 1-4 orders of magnitude compared to the total annihilation or decay rate (e.g. Bergström & Ullio 1997). The unprecedented sensitivity and spectral resolution of the Large Area Telescope (LAT; Gehrels & Michelson 1999; Atwood et al. 2009) aboard the *Fermi Gamma-ray Space Telescope* make it possible to search for dark matter annihilation lines over the whole sky up to a few hundred GeV.

However, other signals can mimic a weak line. Features such as a spectral edge or a broken power law can be mistaken for a line in noisy data, especially when smoothed by the instrumental response. Thus careful separation of diffuse dark matter induced gamma-ray emission from other diffuse sources is crucial.

For example, the recently discovered *Fermi* bubbles extend $\sim 10 \text{ kpc}$ above and below the Galactic center (GC) (Su et al. 2010). Their emission has a flat energy spectrum in $E^2 dN/dE$ from hundreds of MeV to $\sim 100 \text{ GeV}$ implying the ability of the *Fermi* bubbles to accelerate cosmic ray (CR) electrons up to $\sim \text{TeV}$, if the gamma rays are produced by inverse Compton (IC) scattering of the Cosmic Microwave Background (CMB) photons (Su et al. 2010). If there is a spectral break in the *Fermi* bubble spectrum at high energy, the superposition of such a spectrum with other soft-spectrum diffuse components might mimic a bump feature on top of a continuum power law (Profumo & Linden 2012).

In this work, we use 3.7 years data of LAT to study

¹ Institute for Theory and Computation, Harvard-Smithsonian Center for Astrophysics, 60 Garden Street, MS-51, Cambridge, MA 02138 USA

² Physics Department, Harvard University, Cambridge, MA 02138 USA

³ mengsu@cfa.harvard.edu

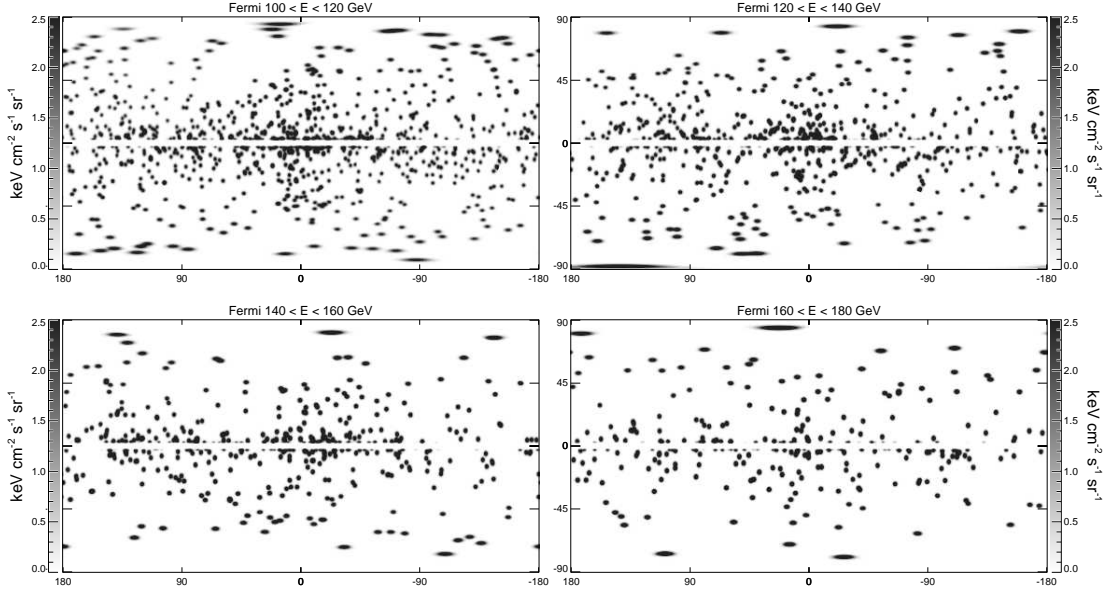


FIG. 1.— All-sky *Fermi*-LAT 3.7 year sky maps in 4 energy bins ranging from 100 to 180 GeV. We use **CLEAN** event class and point sources have been subtracted based on the Second *Fermi*-LAT catalog (2FGL). Large sources, including the inner disk ($-2^\circ < b < 2^\circ, -180^\circ < \ell < 180^\circ$), have been masked. The maps have been smoothed for display with a Gaussian kernel of $\text{FWHM} = 2^\circ$.

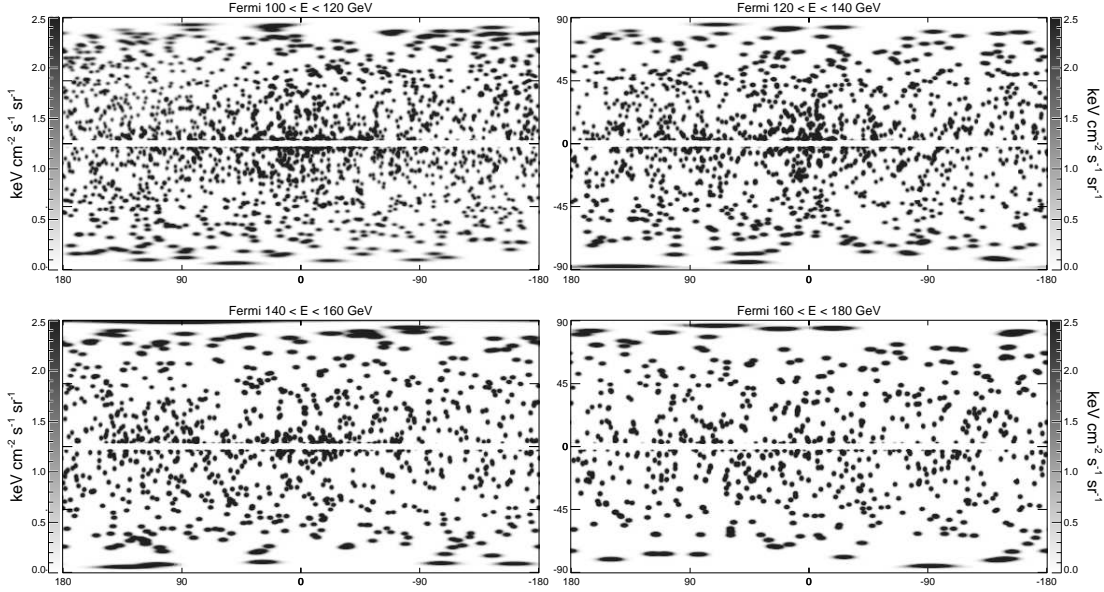


FIG. 2.— Same as Figure 1, but with **SOURCE** class events. This event class contains substantially more background.

the diffuse gamma-ray emission toward the inner Galaxy at $80 < E_\gamma < 200$ GeV. In Section 2 we describe our LAT data selection and map making. In Section 3, we show that the gamma-ray maps reveal a novel gamma-ray cusp toward the Galactic center. We characterize the morphology of the gamma-ray cusp and employ regression template fitting to determine its energy spectrum in Section 4. We performed several validation tests in Section 5. Finally, we discuss our findings and future observations in Section 6.

2. MAP CONSTRUCTION FROM FERMI-LAT DATA

For this project, we constructed full-sky maps from the LAT event files as in our previous work (Dobler et al. 2010; Su et al. 2010; Su & Finkbeiner 2012), except that we now use 3.7 years of Pass 7 (P7_V6) data.

2.1. Fermi Data Selection

The *Fermi* LAT is a pair-conversion telescope, in which incoming photons convert to e^+e^- pairs, which are then tracked through the detector. The arrival direction and energy of each event are reconstructed, and the time of arrival recorded. Event files for every week of the mission

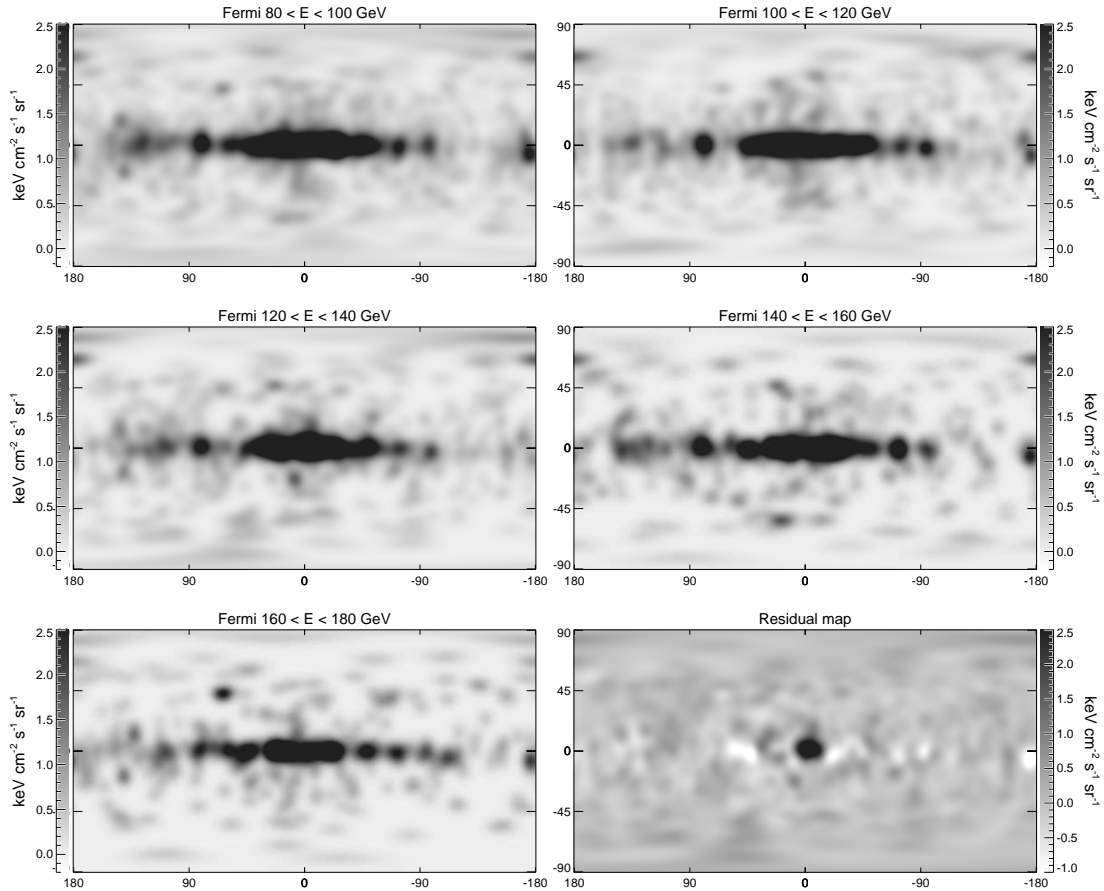


FIG. 3.— All-sky CLEAN 3.7 year maps in 5 energy bins, and a residual map (*lower right*). The residual map is the 120 – 140 GeV map minus a background estimate, taken to be the average of the other 4 maps where the average is computed in $E^2 dN/dE$ units. This simple background estimate is sufficient to remove the Galactic plane and most of the large-scale diffuse structures and even bright point sources. A cuspy structure toward the Galactic center is revealed as the only significant structure in the residual gamma-ray map. All of the maps are smoothed with a Gaussian kernel of $\text{FWHM} = 10^\circ$ without source subtraction.

are available on the Internet, and it is from these files that we build our maps.

The point spread function (PSF) is about 0.8° for 68% containment at 1 GeV and decreases with energy as $r_{68} \sim E^{-0.8}$, asymptoting to $\sim 0.2^\circ$ at high energy. The LAT is designed to survey the gamma-ray sky in the energy range from about 20 MeV to several hundreds of GeV.

We use the latest publicly available data and instrument response functions, known as Pass 7 (P7_V6)⁴. For most figures in this work we use the CLEAN event class, which has larger effective area than ULTRACLEAN and lower background than SOURCE. In a few cases, we show figures made with ULTRACLEAN or SOURCE events as evidence that this choice has no qualitative effect on our results.

Photons coming from the bright limb at Earth’s horizon, dominantly produced by grazing-incidence CR showers in the atmosphere, are a potential source of contamination. We minimize this background by selecting events with zenith angle less than 100° as suggested in

the *Fermi* Cicerone⁵. We also exclude some time intervals, primarily while *Fermi* passes through the South Atlantic Anomaly.

2.2. Map Making

We generate full-sky maps of counts and exposure using HEALPix, a convenient equal-area iso-latitude full-sky pixelization widely used in the CMB community.⁶ Spherical harmonic smoothing is straightforward in this pixelization, and we smooth each map by the kernel required to obtain an approximately Gaussian PSF of some target FWHM, usually 10° . We generate maps for front- and back-converting events separately, smooth them to a common PSF, and then combine them.

We construct maps both with and without point source subtraction. We subtract point sources listed in the Second *Fermi*-LAT catalog (2FGL), which is based on 24 months of P7_V6 LAT observations.⁷ The PSF and ef-

⁵ <http://fermi.gsfc.nasa.gov/ssc/data/analysis/documentation/>.

⁴ Details at http://fermi.gsfc.nasa.gov/ssc/data/analysis/documentation/Pass7_usage.html

⁶ HEALPix software and documentation can be found at <http://healpix.jpl.nasa.gov>, and the IDL routines used in this analysis are available as part of the IDLUTILS product at <http://sdss3data.lbl.gov/software/idlutils>.

⁷ http://fermi.gsfc.nasa.gov/ssc/data/access/lat/2yr_catalog,

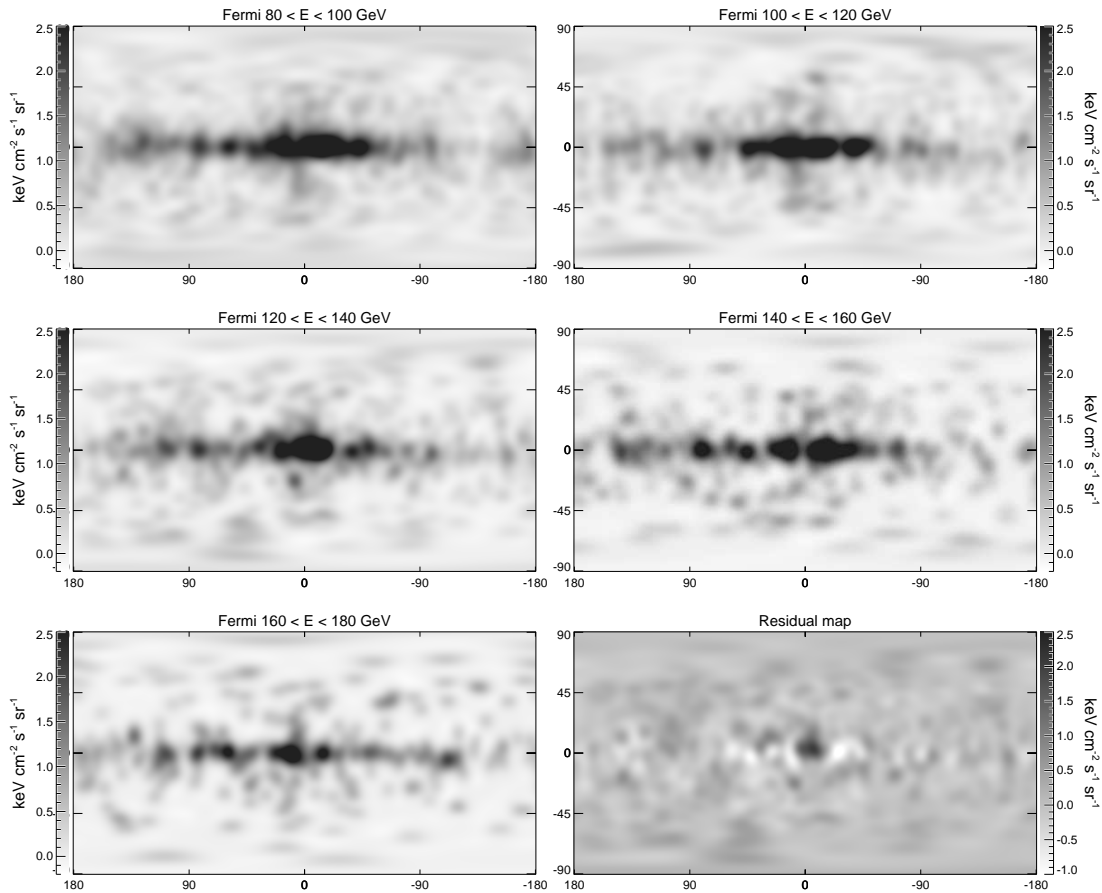


FIG. 4.— The same as Figure 3 but we have subtracted point sources before smooth the maps.

fective area of the *Fermi*-LAT varies with energy, and we subtract each point source from the maps in each energy bin, using the in-flight version of the PSF contained in the P7_V6 IRFs.

For the 400 brightest and 400 most variable sources, the subtraction is noticeably imperfect at lower energies (and we assume it is also at the higher energies used in this work), so we interpolate over the core of the PSF after subtracting the best estimate. We also mask out sources including Geminga, 3C 454.3, and LAT PSR J1836+5925 and large sources like Orion and the Magellanic Clouds as we did in the previous papers (Su et al. 2010; Su & Finkbeiner 2012), although they are unlikely to be a problem at $E > 80$ GeV, where we are searching for lines.

We produce the exposure maps using the `gtltcube` and `gtexpcube2` tasks in the Fermi Science Tools. For bright sources, the exposure is set to zero for excised pixels. For the smoothed maps, both the count map and exposure map are smoothed, and then divided. At high energies, where the PSF is small, this effectively interpolates over the masked pixels.

the file we used is `gll_psc_v07.fit`

3. EVIDENCE FOR RESOLVED GAMMA-RAY CUSP EXCESS AT 120-140 GEV

In Figures 1 and 2, we show the full sky map in four energy bins in the range 100 to 180 GeV, using *CLEAN* and *SOURCE* events, respectively. Even after nearly four years of observation, the number of gamma-ray photons with $E \gtrsim 100$ GeV is still quite limited and the maps are Poisson noise dominated. In order to inspect diffuse gamma-ray structure, we smooth the maps with a Gaussian kernel of $\text{FWHM} = 10^\circ$. Smoothed *CLEAN* maps in various energy bins with $E > 80$ GeV, before and after subtracting point sources, are shown in Figures 3 and 4, respectively. To look for any diffuse gamma-ray emission component with a distinctive energy spectrum, we examine various linear combinations of maps that cancel out the Galactic plane emission and visually inspect the residual maps.

Interestingly, when we subtract the average map (averaged in $E^2 dN/dE$ units) of the 80 – 100 GeV, 100 – 120 GeV, 140 – 160 GeV, and 160 – 180 GeV maps from the 120 – 140 GeV map, most of the large scale diffuse gamma-ray structures (including the relatively bright Galactic plane) and visible point sources have been largely removed. However, a resolved cuspy structure toward the inner Galaxy with a size slightly larger than the

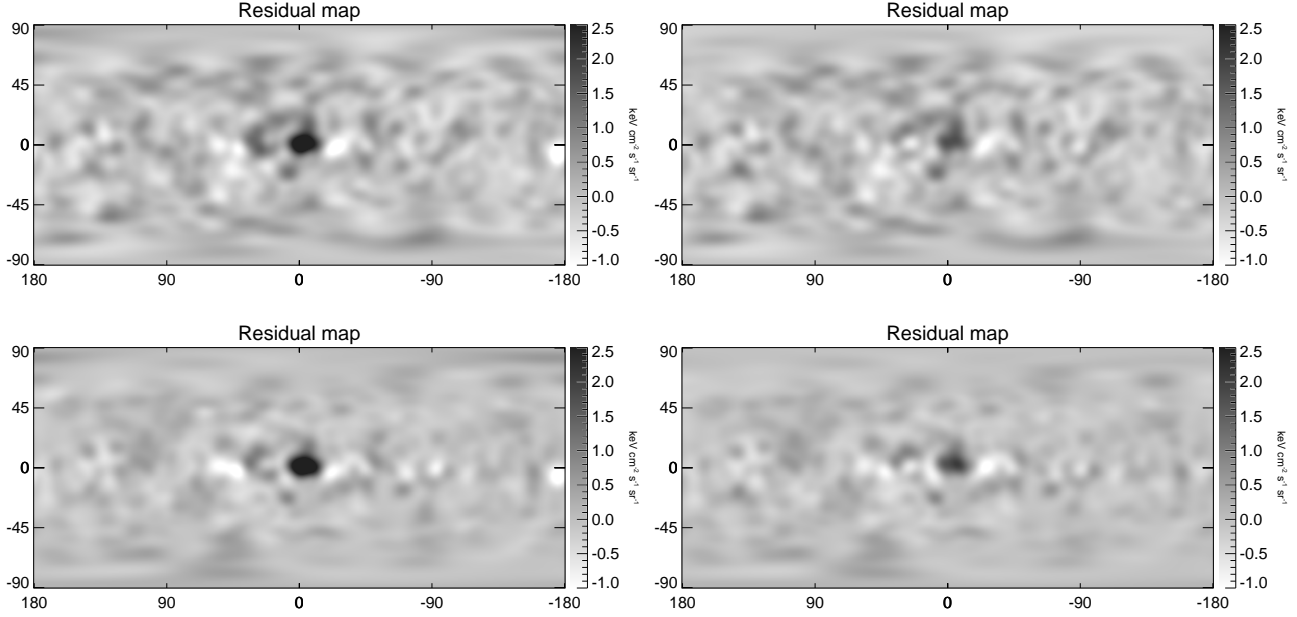


FIG. 5.— Residual maps the same as the *lower right* panel of Figures 3 and 4, but using **SOURCE** events before (*upper left panel*) and after (*upper right panel*) point source subtraction, or using **ULTRACLEAN** events before (*lower left panel*) and after (*lower right panel*) point source subtraction.

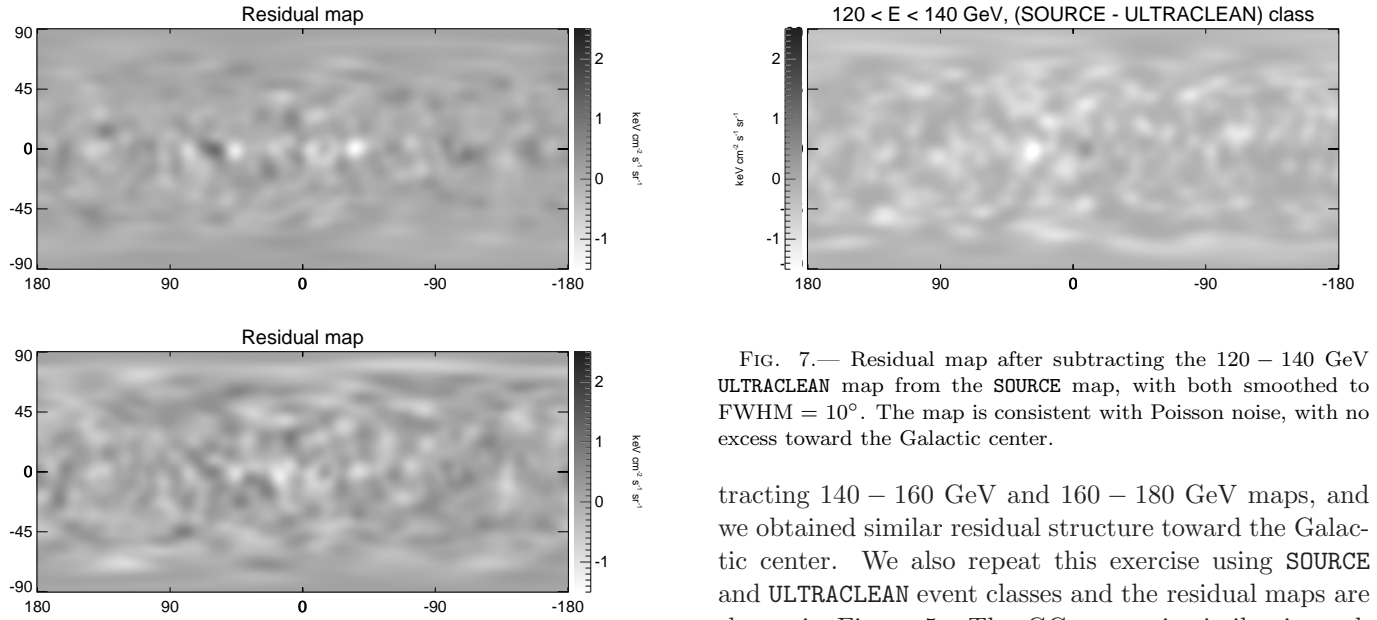


FIG. 6.— Residual maps by subtracting the average map of 100 – 120 GeV and 140 – 160 GeV maps from the average map of 80 – 100 GeV and 160 – 180 GeV maps (individual maps are shown in Figure 3). Most of the large scale diffuse gamma-ray structures (including the Galactic plane) and bright point sources have been removed, and *no* gamma-ray cuspy structure toward the Galactic center is visible in the residual gamma-ray maps. The maps are constructed using *Fermi*-LAT 3.7 year **CLEAN** events (*upper panel*) and **SOURCE** events (*lower panel*), respectively.

smoothing kernel is revealed as the only visible structure in the residual gamma-ray map. We have repeated the analysis only subtracting 80 – 100 GeV and 100 – 120 GeV maps from the 120 – 140 GeV map, or only sub-

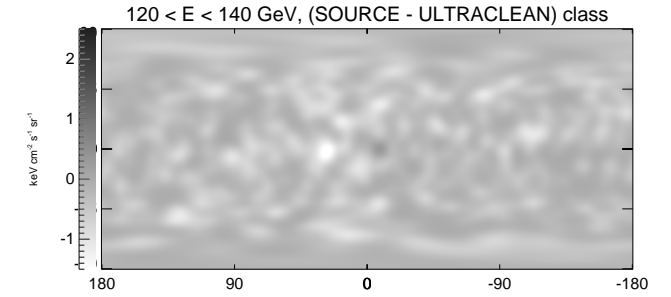


FIG. 7.— Residual map after subtracting the 120 – 140 GeV **ULTRACLEAN** map from the **SOURCE** map, with both smoothed to $\text{FWHM} = 10^\circ$. The map is consistent with Poisson noise, with no excess toward the Galactic center.

tracting 140 – 160 GeV and 160 – 180 GeV maps, and we obtained similar residual structure toward the Galactic center. We also repeat this exercise using **SOURCE** and **ULTRACLEAN** event classes and the residual maps are shown in Figure 5. The GC excess is similar in each case, and the rest of the gamma-ray sky is consistent with Poisson noise. This excess at $\sim 120 - 140$ GeV strongly suggests a novel diffuse gamma-ray component toward the Galactic center with unusual spectrum. Furthermore, this energy range coincides with the recently suggested tentative signature of gamma-ray excess at 130 GeV (Bringmann et al. 2012; Weniger 2012), which is under active debate in the literature (Boyarsky et al. 2012; Tempel et al. 2012; Profumo & Linden 2012). Assuming the distance to the Galactic center is $R_\odot = 8.5$ kpc, the size of the gamma-ray cusp is $\lesssim 1$ kpc.

We show in Figure 6 the difference map between the average map of 80 – 100 GeV and 160 – 180 GeV maps

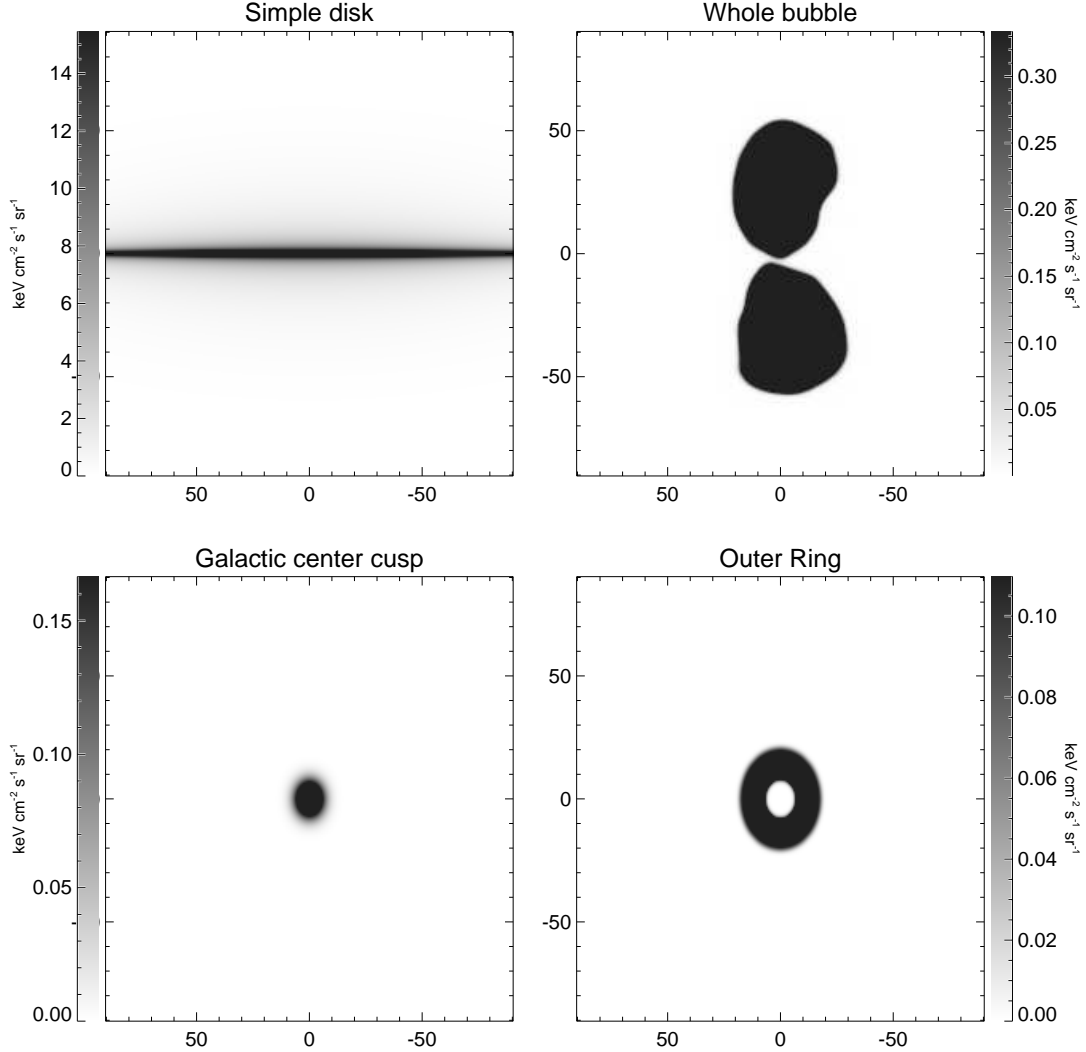


FIG. 8.— Spatial templates used in the Poisson likelihood analysis. *Upper left*: Galactic disk template, *upper right*: *Fermi* bubble template, *lower left*: gamma-ray cuspy template as a Gaussian distribution with $\text{FWHM} = 4^\circ$, *lower right*: outer ring template as a Gaussian distribution with $\text{FWHM} = 10^\circ$, but masking out the central region where the gamma-ray cuspy template is. In Figure 9 and Figure 11, we split the *Fermi* bubble template into two components one with $|b| > 30^\circ$ and the other with $|b| < 30^\circ$.

and the average map of 100 – 120 GeV and 140 – 160 GeV maps. The difference map is consistent with Poisson noise and *no* diffuse gamma-ray excess toward the inner Galaxy is visible. In order to test whether the excess is due to residual cosmic ray contamination, we subtract ULTRACLEAN sky maps from SOURCE sky maps. This residual map should be mostly dominated by cosmic rays since a large fraction of the real gamma-ray photons have been removed. Indeed, Figure 7 demonstrates that there is no excess toward the inner Galaxy in this map, thus we can rule out the possibility that the central excess is due to cosmic ray contamination in the LAT data.

Toward the inner Galaxy, the *Fermi* bubbles extend $\sim 50^\circ$ above and below the Galactic center, with a width of $\sim 40^\circ$ in longitude. The gamma-ray emission associated with these bubbles has a significantly harder spectrum ($dN/dE \sim E^{-2}$) than the inverse Compton emission from electrons in the Galactic disk, or the gamma-

rays produced by decay of π^0 from proton-ISM collisions. We note that the morphology of the resolved gamma-ray cusp has a different shape from the bubbles, and the bubble structure has been largely cancelled out and not visible in the residual maps (as shown in e.g. Figure 5). Thus we conclude that the newly revealed gamma-ray cusp has no obvious connection with the bubbles. We will also demonstrate this more explicitly in Section 4.

4. ENERGY SPECTRUM OF THE GAMMA-RAY CUSP

In §3 we argued for the existence of an excess in the GC at $E = 120 - 140$ GeV, previously noted by Bringmann et al. (2012) and Weniger (2012). This motivates a more careful investigation of the energy spectrum and spatial distribution of the emission.

4.1. Template Regression

As in our previous work (e.g., Su et al. 2010), we consider linear combinations of spatial templates and com-

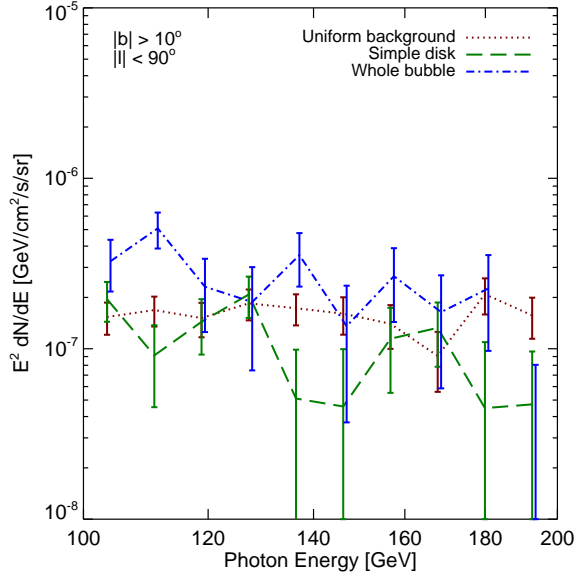


FIG. 9.— Spectral energy distribution of three diffuse gamma-ray templates. The disk-correlated emission (*green dashed*) approximately traces the inverse Compton and bremsstrahlung components. The spectrum of the uniform emission (*dotted brown line*) includes the isotropic part of the extragalactic background and cosmic-ray contamination. We have not included the dust-correlated emission or *Loop I* template as in Su et al. (2010), because the expected spectrum is softer and we do not expect a significant contribution from these components at $E \gtrsim 100$ GeV. Vertical bars show the marginalized 68% confidence range derived from the parameter covariance matrix for the template coefficients in each energy bin.

pute the likelihood that the gamma-ray maps are described by a given linear combination. We fit a coefficient for each emission component using a multi-linear regression of simple templates, one energy bin at a time. This technique provides an estimate of the energy spectrum of each component using as few physical assumptions as possible.

By combining results from 16 logarithmically-spaced energy bands from 85 GeV to 200 GeV, we determine the spectral energy distribution for each component. In each fit, we model the “conventional” emission using three simple templates: a Galactic disk model, the *Fermi* bubbles, and a uniform background. The Galactic disk template has the functional form $(\csc |b|) - 1$ in latitude and is a Gaussian ($\sigma_\ell = 80^\circ$) in longitude, as in Su et al. (2010). The disk model mostly accounts for gamma rays from the Galactic plane including those produced by point sources, ISM emission (π^0 and Bremsstrahlung) and inverse Compton scattering. The uniform background template absorbs the isotropic background due to extra-galactic emission and misclassified charged particle contamination, including heavy nuclei at high energies. We show maps of these templates in Figure 8.

For each set of model parameters, we compute the Pois-

son log likelihood,

$$\ln \mathcal{L} = \sum_i k_i \ln \mu_i - \mu_i - \ln(k_i!), \quad (1)$$

where μ_i is the model counts map (i.e., linear combination of templates times exposure map) at pixel i , and k is the map of observed counts. The last term is a function only of the observed maps. We compute parameter errors in the Gaussian approximation by inverting the matrix of second partial derivatives of $-\ln \mathcal{L}$ to obtain the covariance matrix, and taking the square root of the diagonals. The 1σ Gaussian error corresponds to $\Delta \ln \mathcal{L} = 1/2$.

Template-correlated spectra for the 3-template fit are shown in Figure 9. The energy spectra show no significant deviation from a power law for any of the three components. This fact, together with the distinct spatial morphology of the gamma-ray cusp suggests the need to include a cusp template (shown in Figure 8) in the model. Inclusion of this template barely alters the derived spectrum of the first three components, but yields significant coefficients for the cusp from 110 to 140 GeV (Figure 10 and Table 1). The fact that the bubble coefficients show no such bump indicates that the bubble structure is unrelated to the ~ 130 GeV excess. We find that the surface brightness of the center of the cusp is nearly two orders of magnitude greater than that of the *Fermi* bubble structure, but only over a limited energy range.

In Figure 10, we have done the fit with two different spatial masks: one excludes $|b| < 1^\circ$ to avoid contamination from the Galactic disk close to the plane and the Galactic center (including the Galactic “ridge”); another one excludes much more of the Galactic disk with $|b| < 5^\circ$ and $|l| > 6^\circ$ without masking the Galactic center region. We have obtained similar results for both data cuts. Given the energy resolution of the *Fermi*-LAT at $E \gtrsim 100$ GeV, the spectral excess at $110 \lesssim E \lesssim 140$ GeV is consistent with emission from one or two lines after considering the line-spread function (LSF) (Edmonds 2011), which strongly suggests the novel nature of the gamma-ray cusp as no known astrophysical process can produce this feature. Except for unexpected instrumental systematics or an increasingly unlikely statistical fluke, a dark matter annihilation signal from the inner Galaxy is the most likely explanation.

In another variant of the fit, we split the bubble template into two independent components in the fitting, high latitude ($|b| > 30^\circ$) and low latitude ($|b| < 30^\circ$). The purpose is to demonstrate that the low latitude bubble is also independent from the gamma-ray cusp. Again, we find no sign of a bump in the spectra of other diffuse gamma-ray components, but the cusp has a spectrum with an excess at 110 – 140 GeV and is consistent with zero in the other bins (Figure 11). Instead of using CLEAN class, we have tried using SOURCE class for the likelihood analysis, and obtained similar results (Figure 12).

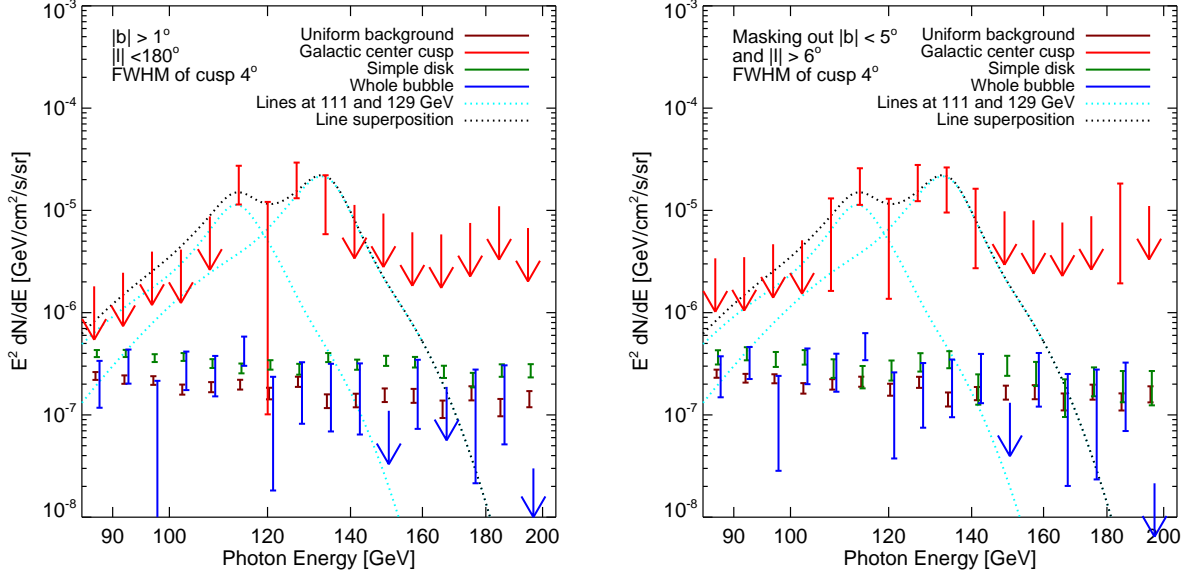


FIG. 10.— *Left panel:* Spectral energy distributions of the templates listed in the figure legend. In the *left panel*, we use CLEAN events with $|b| > 1^\circ$ and all longitudes. Besides the disk-correlated emission (*green*), uniform emission (*brown*), and the *Fermi* bubble template (*blue*), the cusp component modeled as a $\text{FWHM} = 4^\circ$ Gaussian in the GC (*red*) has been included. Vertical bars show the marginalized 68% confidence range derived from the parameter covariance matrix for the template coefficients in each energy bin. Arrows indicate 1σ upper limits. For reference, we overplot lines centered at 111 GeV and 129 GeV (*dotted cyan*) convolved with a three-Gaussian approximation of the LAT instrumental response (Edmonds 2011), and their sum (*dotted black*). The line centers and amplitudes are determined from a fit to the spectrum in the right panel (see text). *Right panel:* the same as the left panel but using data masking out $|b| < 5^\circ$ and $|l| > 6^\circ$.

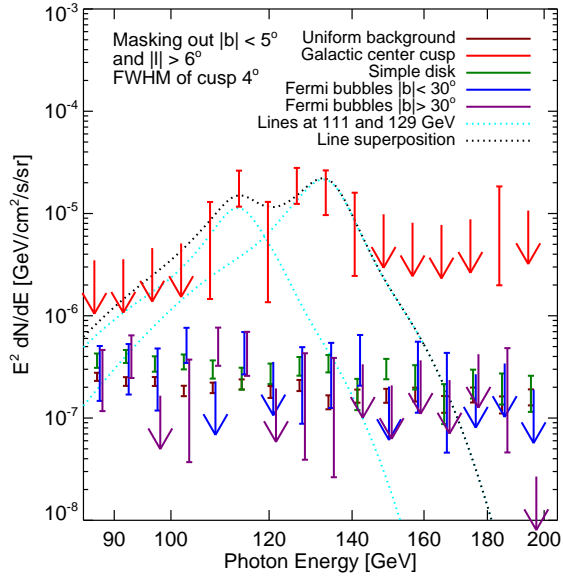


FIG. 11.— Same as right panel of Figure 10 but splitting the bubble template into two regions one with $|b| > 30^\circ$ and the other with $|b| < 30^\circ$.

The gamma-ray cusp appears to possess a symmetric distribution around the Galactic center. To investigate whether there is any more extended cusp component contributing the excess at 120 – 140 GeV, we include an extra “outer ring” template as shown in Figure 8. The outer ring template is a $\text{FWHM}=10^\circ$ Gaussian with an 8° radius hole in the center. Even with this freedom,

E range (GeV)	Energy	cusp (CLEAN)	cusp (SOURCE)
84.9 – 89.5	87.2	-1.01 ± 4.42	-2.19 ± 4.30
89.5 – 94.5	92.0	-0.79 ± 4.28	-1.53 ± 4.29
94.5 – 99.7	97.1	0.03 ± 4.64	4.37 ± 5.26
99.7 – 105.2	102.4	0.06 ± 5.04	3.05 ± 5.77
105.2 – 111.0	108.1	7.37 ± 5.73	8.61 ± 5.95
111.0 – 117.1	114.0	18.58 ± 7.25	21.80 ± 7.57
117.1 – 123.6	120.3	7.18 ± 5.82	7.19 ± 6.03
123.6 – 130.4	127.0	20.06 ± 7.75	19.78 ± 7.61
130.4 – 137.6	134.0	17.91 ± 8.38	10.82 ± 7.83
137.6 – 145.2	141.4	9.50 ± 6.78	16.71 ± 7.50
145.2 – 153.2	149.2	4.07 ± 5.73	3.07 ± 5.36
153.2 – 161.7	157.4	1.70 ± 6.29	8.07 ± 7.14
161.7 – 170.6	166.1	3.11 ± 4.50	4.34 ± 4.88
170.6 – 180.1	175.2	3.08 ± 5.69	2.91 ± 5.90
180.1 – 190.0	185.0	10.11 ± 8.18	7.07 ± 8.34
190.0 – 200.5	195.2	3.99 ± 7.04	1.84 ± 6.46

TABLE 1
THE TEMPLATE FITTING COEFFICIENTS AND ERRORS OF THE DIFFUSE GAMMA-RAY CUSP CORRESPOND TO THE RIGHT PANEL OF FIGURE 10 AND RIGHT PANEL OF FIGURE 12. THE GAMMA-RAY LUMINOSITY IN EACH ENERGY RANGE IS SHOWN IN THE UNIT OF $\text{keV cm}^{-2} \text{s}^{-1} \text{sr}^{-1}$.

there is no significant change in the cusp spectrum (Figure 14). There was no significant improvement of the likelihood for this model, and the spectrum of the outer ring is consistent with zero. Our conclusion is that the gamma-ray cusp is a distinct component, and is centrally concentrated.

4.2. Trials factor

We use a trials factor of 300 for this bump. This is based on the fact that the LAT energy resolution is \sim

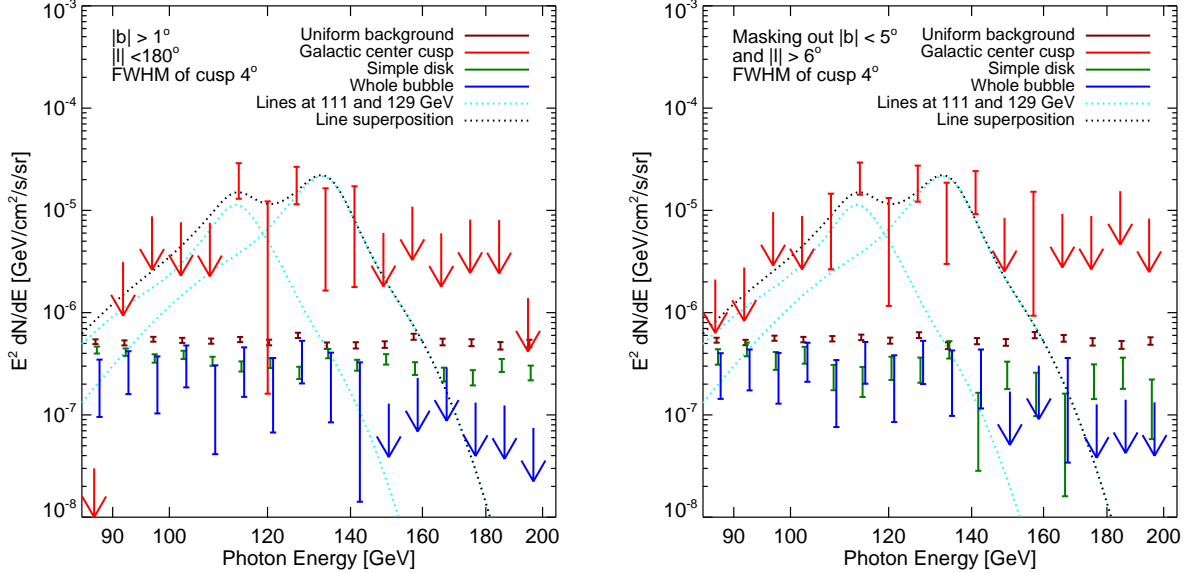


FIG. 12.— Same as Figure 10 but using SOURCE events instead of CLEAN. The level of the uniform background is more than a factor of 2 higher than that shown in Figure 10. However, the resulting energy spectrum of the gamma-ray cusp (red dashed line) is quite similar to that shown in figures 10 and 11.

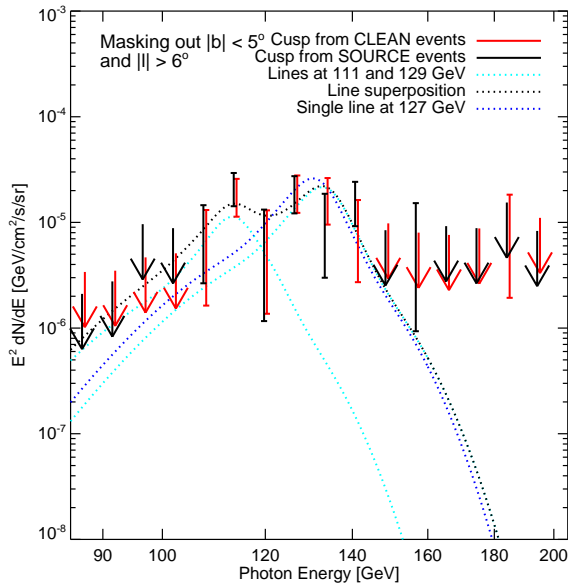


FIG. 13.— Same as right panel of Figure 10 but overplot the best fit one gamma-ray line profile convolved with the instrument response, and compared with the best fit two-line profile.

10% over most of the energy range, and a line anywhere from 1 to 300 GeV would have been just as impressive. Furthermore, a wider lines (or two lines near each other) has an additional trials factor. We allow an extra factor of 5, giving us 300.

The raw significance of the spectral feature is 5.0σ , obtained by summing the significance of each bin in quadrature (Table 1). After diluting the p value corresponding to 5.0σ by a factor of 300, we obtain a significance corresponding to 3.7σ . We note that, if the line is real, an additional 40% more data will be enough to obtain a 5.0σ

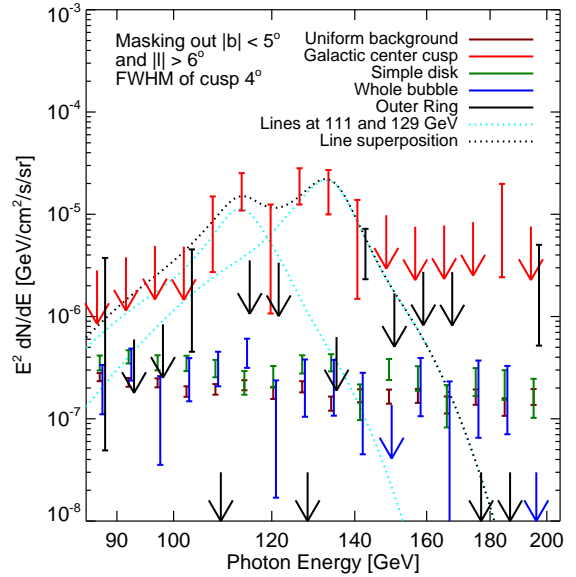


FIG. 14.— Same as right panel of Figure 10 but including extra outer ring template.

detection, even with the trials factor of 300. This additional data could come from waiting until late 2013, or by improved analysis (perhaps in Pass 8) that recovers more events (e.g. photons that convert in the calorimeter).

5. VALIDATION TESTS

5.1. Assessment of Line Profile

In the previous section, we investigated the cusp emission by analyzing maps in various energy bins. This allowed a separation of spectral components by morphology, but relied on an arbitrary choice of binning. The

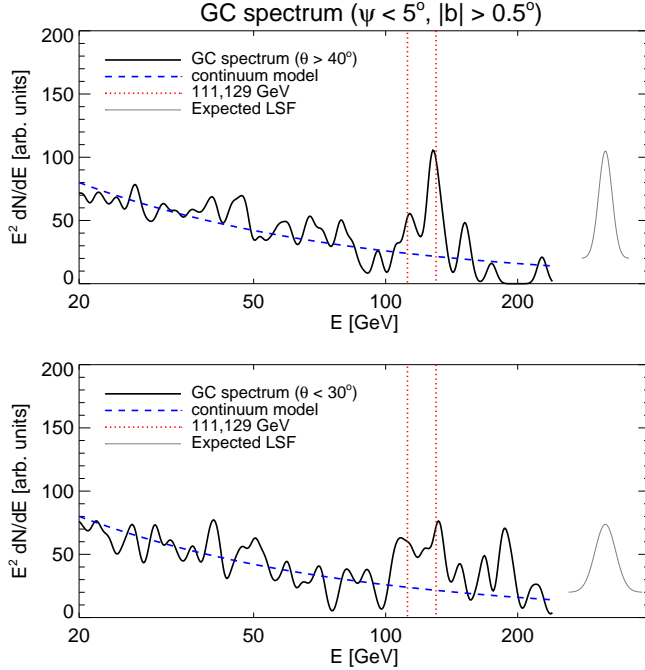


FIG. 15.— Spectrum of emission within 5° of the Galactic center, excluding $|b| < 0.5^\circ$. High-incidence angle events (*upper panel*) have a factor of ~ 2 better energy resolution than those that enter the LAT close to normal incidence (*lower panel*). Both spectra have been smoothed by a Gaussian of 0.06 FWHM in $\Delta E/E$, similar to the expected resolution of the upper panel.

result – that there is a cusp of emission in the inner Galaxy – motivates an unbinned analysis of this region.

In an unbinned analysis, one dispenses with arbitrary binning choices (size and shift) and instead analyzes individual photon events. For example, the parameters of a well defined model may be estimated with no binning in space or energy. In the absence of a principled model, a compromise technique is to convolve a finely binned energy histogram with some kernel and compare profiles of prospective lines with those expected for a true line, i.e. the instrumental response convolved with the smoothing kernel.

In the case of LAT data this presents an interesting opportunity. Energy resolution of events at high incidence angle ($\theta \sim 60^\circ$) is a factor of ~ 2 better than that of normal-incidence photons. This allows the following test.

We select low incidence ($\theta < 30^\circ$) and high incidence ($\theta > 40^\circ$) samples. Restrict to those near the GC ($\psi < 5^\circ$) but not in the plane ($|b| < 0.5^\circ$). Convolve each with a kernel and compare them (Figure 15). We adopt an LSF with a FWHM of $\Delta E/E = 0.06$ for high incidence and 0.12 for low incidence (Edmonds 2011), and in both cases convolve with another FWHM 0.06 Gaussian. After convolution, the LSF is FWHM 0.085 for high incidence and 0.134 for low incidence. Normalized Gaussians of these widths are shown for reference, normalized to the expected line strength at 130 GeV. Maps constructed using only high incidence events are

shown in Figure 16.

Note that:

- The 129 GeV feature shape is strikingly similar to that expected for a line. The 111 GeV feature is marginal but is also compatible with a line.
- Noise can be sharper than the LSF but real signal is not. Many spikes appear that are not real.
- In other cases, fluctuations appear, but are not present in both low and high incidence spectra.

This analysis did introduce some additional parameters, but we have made natural choices for them: The 68% containment radius of the cusp is approximately 5° , the Galactic ridge is about 0.5° thick, and the $\Delta E/E = 0.06$ smoothing kernel is similar to the LSF of the LAT at high incidence. Smoothing a spectrum by its LSF is often a good compromise between resolution and noise suppression in the high-noise limit. Because these parameters are all fixed to natural values, there is no significant trials factor for this test, apart from the obvious one, that the lines could have appeared anywhere (Section 4.2).

This test did not have to succeed. The fact that the high-incidence photon sample has sharper spectral features is important; if the spectra in Figure 15 had been reversed, it would have been devastating for the line hypothesis.

5.2. Null test: Galactic plane spectrum

To emphasize that the line feature in Figure 15 appears near the Galactic center and not elsewhere, we perform the same analysis on the Galactic plane ($|b| < 2^\circ$) away from the GC ($\psi > 5^\circ$). We find no indication of a line in either high-incidence or low-incidence photons (Figure 17).

5.3. Null test: Albedo photons

Another null test is provided by the Earth albedo photons. Cosmic-ray induced cascades in the Earth's atmosphere shower photons on the LAT at high zenith angle ($Z > 108^\circ$). These provide another null test, as there is no reason for there to be a 130 GeV feature in the albedo spectrum. On average, no feature is seen (Figure 18). However, there is a hint of a line at 130 GeV in the low-incidence events and one at 111 GeV in the high-incidence events. These features also require a trials factor, but if they turn out to be robust, then serious concerns would be raised about instrumental artifacts giving rise to the observed lines.

6. DISCUSSION AND CONCLUSION

Morphology: Using data from 3.7 year observations by *Fermi*-LAT, we have identified a resolved gamma-ray cusp structure toward the Galactic center region. We first take a linear combination of smoothed maps

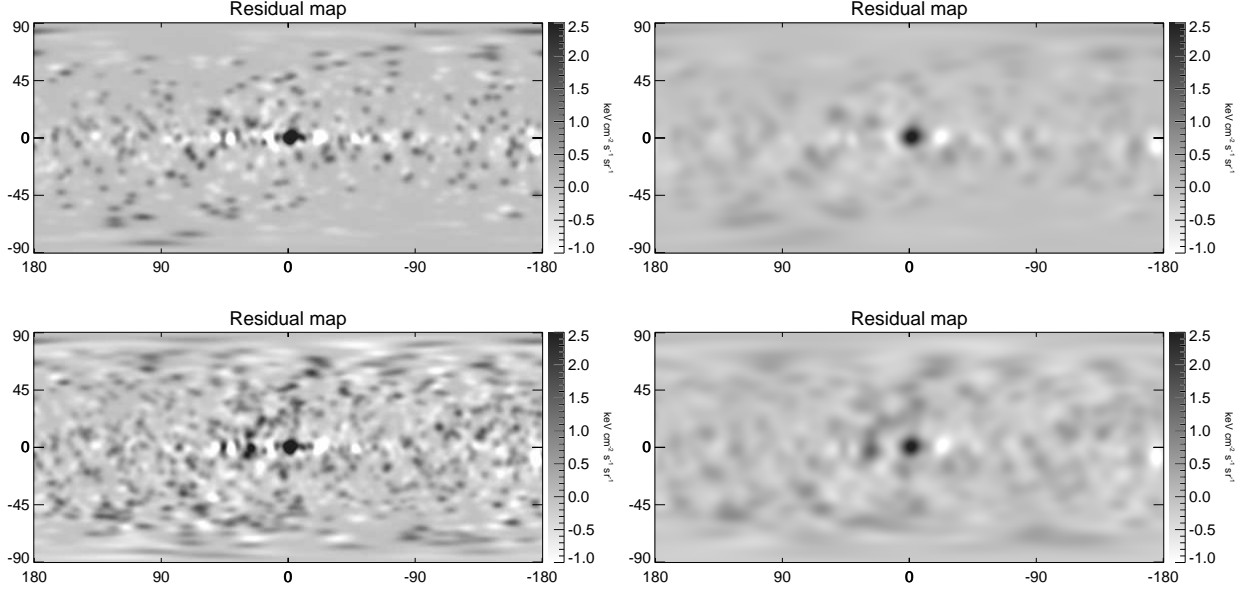


FIG. 16.— Same as Figure 5, but using only events with high incidence angle $\theta > 40^\circ$ which has better energy resolution. The maps have been smoothed to 5° (left two panels) and 10° (right two panels), and using CLEAN event class (upper two panels) and SOURCE event class (lower two panels). The resolved gamma-ray cusp structure is concentrated toward the Galactic center.

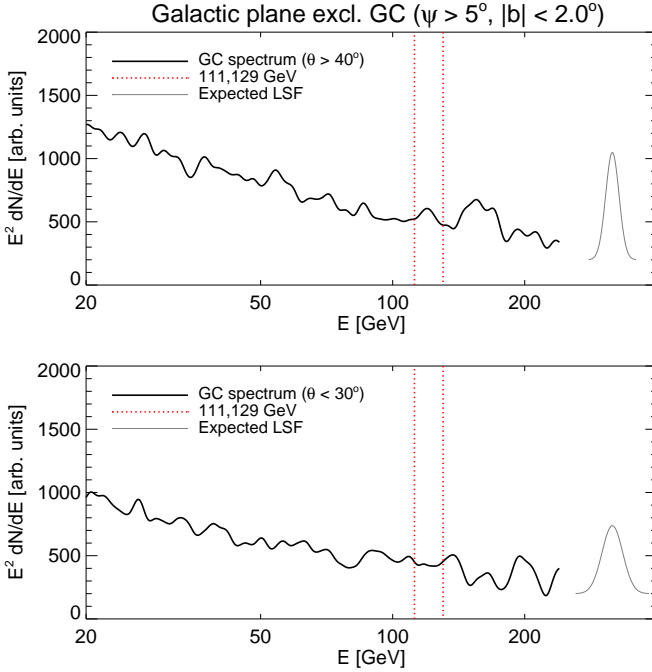


FIG. 17.— Like Figure 15, except for $|b| < 2^\circ$ excluding photons within 5° of the Galactic center. There is no indication of a spectral feature near 130 GeV in the Galactic plane away from the Galactic center.

that cancels out continuum emission and reveals the cusp structure in a model-independent way. We find that this structure only appears in energy range from ~ 120 GeV to ~ 140 GeV after searching $80 < E < 200$ GeV maps. The FWHM of the cusp morphology, if modeled with a Gaussian, is $\lesssim 4^\circ$ and is unrelated to the *Fermi* bubble structure (in contrast to Profumo & Linden 2012). No other region of the sky reveals any significant excess in

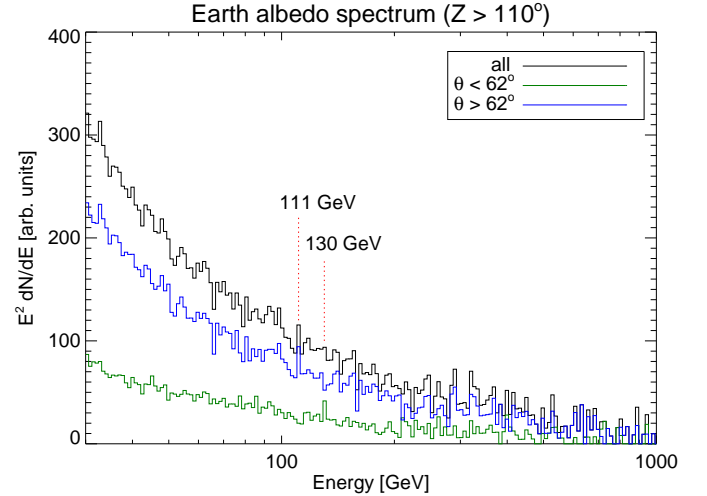


FIG. 18.— Photons from cascades in the Earth's atmosphere (“albedo” photons) show a slight excess at 111 and 130 GeV also. Because these photons arrive at high zenith angle ($Z > 110^\circ$), they tend to have a high incidence angle (median $\theta = 63.2^\circ$). The low- θ photons show a small bump at 130 GeV, and the high- θ photons show a small bump at 111 GeV. The cuts were chosen to maximize these features, so interpretation of this plot requires a modest trials factor.

this energy range.

Template regression: We perform a Poisson likelihood analysis to obtain the energy spectrum of the diffuse gamma-ray cusp. We have modeled the diffuse gamma-ray emission by a combination of templates including the cusp template, a uniform gamma-ray background, a thin gamma-ray disk tracing the Galactic plane, and the *Fermi* bubble structure. By modeling the data with a linear combination of templates and maximizing the Poisson likelihood of observing the observed counts, we

are able to separate the cusp emission from the *Fermi* bubbles and the Galactic disk. Inasmuch as the template is actually correct, this “matched filter” gives an optimal estimate of the flux in each energy bin. The uncertainty estimates include marginalizing over the uncertainty in the other templates we used to fit the data. We do not make *a priori* assumptions about the dark matter profile. We find that the cusp emits gamma rays with a luminosity of $(3.2 \pm 0.6) \times 10^{35}$ erg/s, or $(1.7 \pm 0.4) \times 10^{36}$ photons/sec. The null hypothesis of zero intensity is ruled out by 5.0σ (3.7σ with trials factor).

Line profile: The energy spectrum of this novel cusp structure at $E \gtrsim 80$ GeV is consistent with a single spectral line (at energy 127.0 ± 2.0 GeV with $\chi^2 = 4.48$ for 4 d.o.f.) convolved by the LAT energy response (Rajaraman et al. 2012). A pair of lines at 110.8 ± 4.4 GeV and 128.8 ± 2.7 GeV provides a marginally better fit (with $\chi^2 = 1.25$ for 2 d.o.f.). The observation is compatible with a 142 GeV WIMP annihilating through γZ and γh for $m_h \sim 130$ GeV, as in the “Higgs in Space” scenario (Jackson et al. 2010). Given the properties of the resolved gamma-ray cusp, and assuming it originates from matter annihilation, constraints on the dark matter density profile and annihilation rate or cross section of dark matter can be placed to different models (e.g. Goodman et al. 2011; Jackson et al. 2010; Cline 2012; Bertone et al. 2009). At present, the extrapolation from the local dark matter density into the Galactic center is uncertain enough that there are large uncertainties in the cross section. We do not attempt to improve those estimates in this work.

Comparison to previous work: The recent study by M. Ackermann et al. (2012) put constraints on line emission from the inner Galaxy, excluding photons within $|b| < 5^\circ$. Therefore, their constraints are not in conflict with the signal claimed in this paper, which is mostly within 5° of the GC. Ackermann et al. searched for dark matter gamma-ray line signal from 4.8 GeV to 264 GeV, updating the results from the earlier study with 11 months *Fermi*-LAT data (Abdo et al. 2010). The results from this study are obtained from two years of *Fermi*-LAT data and used the Pass 6 processing, which has somewhat worse background and instrumental systematics compared to Pass 7.

The Galactic center is known to be a region with diffuse high energy gamma-ray emission (Aharonian et al. 2006a), especially the Galactic center ridge (Aharonian et al. 2006b). High energy gamma rays are produced by cosmic rays interacting with interstellar gas or giant molecular clouds in the central ~ 200 parsecs. We note that the resolved cusp is

incompatible with a point source given that it extends to $\sim 4^\circ$. To check for contribution from unresolved point sources, we have repeated our analyses masking out regions with $|b| < 1^\circ$, and have obtained similar results, confirming that the cusp is not associated with the Galactic ridge.

The next version of *Fermi*-LAT data (Pass 8) will move us closer to realizing the full scientific potential of the LAT (Atwood 2012). The expected improvements include greatly reduced backgrounds, increased effective area, reduced point-spread function, better understanding of the systematic uncertainties, and particularly extending the energy reach to higher photon energy. Finally, the calorimeters of LAT have been demonstrated to effectively operate as a standalone instrument providing imaging of the sky at $E \gtrsim 10$ GeV, albeit with worse image resolution (at the level of 1°) with a large potential increase in the effective area at high energy and large angle (Atwood 2012). Such data would be valuable for future studies of the gamma ray line(s).

Future study of diffuse gamma rays from the Galactic center region with the improved *Fermi*-LAT data products would be able to better constrain the morphology of the gamma-ray cusp and study in detail the line emission in $120 \lesssim E \lesssim 140$ GeV. With more and better calibrated photon counts, we might be able to reveal the nature of the excess at ~ 130 GeV, e.g. whether the excess is due to single annihilation line or more. The gamma-ray excess in $120 \lesssim E \lesssim 140$ GeV is the first line structure found in gamma rays and strongly suggests the origin from dark matter particle annihilation/decay. We note that detailed imprint of WIMP annihilation can in principle reveal features like WIMP spin and/or other particles in the dark sector. Besides the Galactic center region which provides an ideal nearby laboratory to search for indirect evidence of dark matter, gamma-ray line signatures from dark matter subhalos or galaxy clusters might be also visible at the same energy range. Future work is needed in these areas.

Acknowledgments: We thank Neal Weiner and Tracy Slatyer for helpful discussions. We acknowledge the use of public data from the *Fermi* data archive at <http://fermi.gsfc.nasa.gov/ssc/>. This work would not be possible without the work of hundreds of people, over many years, to design, build, and operate *Fermi*. M.S. and D.P.F. are partially supported by the NASA Fermi Guest Investigator Program. This research made use of the NASA Astrophysics Data System (ADS) and the IDL Astronomy User’s Library at Goddard (Available at <http://idlastro.gsfc.nasa.gov>).

REFERENCES

- Abdo, A. A. et al. 2010, Phys. Rev. Lett., 104, 091302
 Abramowski, A. et al. 2011, Physical Review Letters, 106, 161301, 1103.3266
 Ackermann, M. et al. 2011, Physical Review Letters, 107, 241302, 1108.3546
 Aharonian, F. et al. 2006a, Physical Review Letters, 97, 221102, arXiv:astro-ph/0610509

- . 2006b, *Nature*, 439, 695, arXiv:astro-ph/0603021
- Atwood, W. 2012, in *American Astronomical Society Meeting Abstracts*, Vol. 219, American Astronomical Society Meeting Abstracts, 145.18
- Atwood, W. B. et al. 2009, *ApJ*, 697, 1071, 0902.1089
- Bergström, L. 2000, *Reports on Progress in Physics*, 63, 793, arXiv:hep-ph/0002126
- Bergström, L., & Ullio, P. 1997, *Nuclear Physics B*, 504, 27, arXiv:hep-ph/9706232
- Bergström, L., Ullio, P., & Buckley, J. H. 1998, *Astroparticle Physics*, 9, 137, arXiv:astro-ph/9712318
- Bertone, G., Hooper, D., & Silk, J. 2005, *Phys. Rep.*, 405, 279, arXiv:hep-ph/0404175
- Bertone, G., Jackson, C. B., Shaughnessy, G., Tait, T. M. P., & Vallinotto, A. 2009, *Phys. Rev. D*, 80, 023512, 0904.1442
- Boyarsky, A., Malyshev, D., & Ruchayskiy, O. 2012, *ArXiv e-prints*, 1205.4700
- Bringmann, T., Huang, X., Ibarra, A., Vogl, S., & Weniger, C. 2012, *ArXiv e-prints*, 1203.1312
- Cline, J. M. 2012, *ArXiv e-prints*, 1205.2688
- Dobler, G., Finkbeiner, D. P., Cholis, I., Slatyer, T., & Weiner, N. 2010, *ApJ*, 717, 825, 0910.4583
- Edmonds, Y. V. 2011, PhD thesis, Stanford University
- Gehrels, N., & Michelson, P. 1999, *Astropart. Phys.*, 11, 277
- Gondolo, P., & Silk, J. 1999, *Physical Review Letters*, 83, 1719, arXiv:astro-ph/9906391
- Goodman, J., Ibe, M., Rajaraman, A., Shepherd, W., Tait, T. M. P., & Yu, H.-B. 2011, *Nuclear Physics B*, 844, 55, 1009.0008
- Hooper, D., & Profumo, S. 2007, *Phys. Rep.*, 453, 29, arXiv:hep-ph/0701197
- Jackson, C. B., Servant, G., Shaughnessy, G., Tait, T. M. P., & Taoso, M. 2010, *JCAP*, 4, 4, 0912.0004
- M. Ackermann et al. 2012, *ArXiv e-prints*, 1205.6474
- Profumo, S., & Linden, T. 2012, *ArXiv e-prints*, 1204.6047
- Rajaraman, A., Tait, T. M. P., & Whiteson, D. 2012, *ArXiv e-prints*, 1205.4723
- Su, M., & Finkbeiner, D. P. 2012, *ArXiv e-prints*, 1205.5852
- Su, M., Slatyer, T. R., & Finkbeiner, D. P. 2010, *ApJ*, 724, 1044, 1005.5480
- Tempel, E., Hektor, A., & Raidal, M. 2012, *ArXiv e-prints*, 1205.1045
- Weniger, C. 2012, *ArXiv e-prints*, 1204.2797